Electronic Supplementary Material (ESI) for New Journal of Chemistry.

Supporting Information

A europium (III)-based metal-organic framework as a naked-eye and fast response luminescence sensor for acetone and ferric iron

Jian Wang, Jingru Wang, Yang Li, Min Jiang, Lingwen Zhang and Pengyan Wu*

School of Chemistry and Chemical Engineering & Jiangsu Key Laboratory of Green Synthetic Chemistry for Functional Materials, Jiangsu Normal University, Xuzhou, Jiangsu, 221116, P. R. China;

E-mail: wpyan@jsnu.edu.cn

1. Materials and Methods.

All chemicals were of reagent grade quality obtained from commercial sources and used without further purification. Biphenyl-2,2'-dicarboxylic acid was purchased from Jinan Henghua Sci. & Tec. Co., Ltd., $Eu(NO_3)_3 \cdot 6H_2O$ was purchased from Alfa Aesar, $Fe(NO_3)_3 \cdot 9H_2O$ and the other metal salts were provided from Shanghai Fourth Chemical Reagent Company (China). Stock solution (2×10^{-2} M) of the aqueous nitrate salts of Li^+, Na^+, K^+, Mg^{2+}, Ca^{2+}, Sr^{2+}, Ba^{2+}, Co^{2+}, Ni^{2+}, Cu^{2+}, Mn^{2+}, Zn^{2+}, Cd^{2+}, Ag^+, Hg^{2+}, Pb^{2+}, Al^{3+}, Cr^{3+}, Fe^{3+} and ferrous sulfate were prepared for further experiments. The elemental analyses of C, H and N were performed on a Vario EL III elemental analyzer. X-Ray powder diffraction (XRD) patterns of the Eu−**BPDA** and relative immersed compounds were recorded on a Rigaku D/max-2400 X−ray powder diffractometer (Japan) using Cu-*K*α (λ = 1.5405 Å) radiation. Thermogravimetric analysis (TGA) was carried out at a ramp rate of 5 °C/min in a nitrogen flow with a Mettler-Toledo TGA/SDTA851 instrument. FT-IR spectra were recorded as KBr pellets on Bruker Optics TENSOR 27 FT-IR spectrophotometer. The Eu^{3+} content before or after treated with Fe^{3+} in water were measured by Inductively Coupled Plasma Spectrometer (Perkin Elmer). The solution fluorescent spectra were measured on Hitachi F-4600. Both excitation and emission slit widths were 2.5 nm. The Eu−**BPDA** emulsion was prepared by introducing 1 mg of Eu−**BPDA** powder into 3.00 mL of pure water, the intensity was recorded at 614 nm, excitation at 295 nm. For metal ions' detection, the high concentration of stock solutions of related metal ions (2.0×10^{-2} M) were prepared directly in water solvents.

2. X-ray Crystallography (Single-crystal diffraction) and Characterizations.

2.1 Crystal data of Eu−BPDA:

$C_{21}H_{14}O_7Eu$, Mr = 530.28, Monoclinic, space group *C*2/*c*, *a* = 20.923(5), *b* = 21.410(5), *c* = 8.2496(19) Å, α = 90.00, β = 104.003(3), γ = 90.00, *V* = 3585.8(14) $Å^3$, *Z* = 8, *D*c = 1.965 g cm^{-3}, μ(Mo-Kα) = 0.71073 mm^{-1}, *T* = 153(2) K. 8745 unique reflections [R_{int} = 0.0264]. Final R_1[with $I > 2\sigma(I)$] = 0.0240, wR_2(all data) = 0.0653, GOOF = 0.987. CCDC number: 1035886.

2.2 Crystallography:

Intensities were collected on a Bruker SMART APEX CCD diffractometer with graphitemonochromated Mo-Kα (λ = 0.71073 Å) using the SMART and SAINT programs. The structure was solved by direct methods and refined on F^2 by full-matrix least-squares methods with SHELXTL *version* 5.1. Non-hydrogen atoms of the ligand backbones were refined anisotropically. Hydrogen atoms within the ligand backbones were fixed geometrically at calculated positions and allowed to ride on the parent non-hydrogen atoms.

2.3 Figure S1 (a) The constitutive/constructional fragments composed of H_2**BPDA** and Eu^{III} ion along *b* direction. (b) Coordination polyhedron of the Eu^{III} ion in the structure of Eu−**BPDA**. Symmetry codes: A:-x, y, 0.5-z; B: x, y, 1+z; C: x, y, -1+z; D: -x, y, 1.5-z.

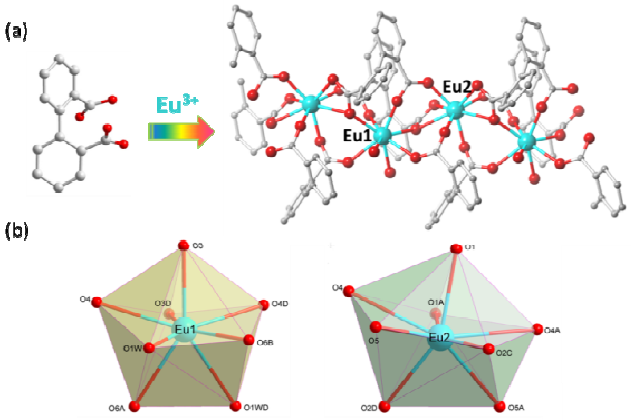

2.4 Selective bond distance (Å) and angle (°) in Eu−**BPDA**.

Eu(1)–O(3D)	2.291(2)	Eu(1)–O(6B)	2.469(2)
Eu(1)–O(3)	2.291(2)	Eu(1)–O(6)	2.469(2)
Eu(1)–O(4D)	2.459(2)	Eu(1)–O(1W)	2.507(3)
Eu(1)–O(4)	2.459(2)	Eu(1)–O(1WD)	2.507(3)
Eu(2)–O(1)	2.313(2)	Eu(2)–O(5)	2.415(3)
Eu(2)–O(1A)	2.313(2)	Eu(2)–O(5A)	2.415(3)
Eu(2)–O(2C)	2.319(2)	Eu(2)–O(4)	2.609(2)
Eu(2)–O(2D)	2.319(2)	Eu(2)–O(4A)	2.609(2)
O(3D)–Eu(1)–O(3)	86.76(13)	O(6B)–Eu(1)–O(6)	108.12(1)
O(3D)–Eu(1)–O(4)	78.31(9)	O(3D)–Eu(1)–O(1W)	147.07(9)
O(3)–Eu(1)–O(4)	71.99(8)	O(3)–Eu(1)–O(1W)	93.61(1)
O(3D)–Eu(1)–O(4D)	71.99(8)	O(4)–Eu(1)–O(1W)	70.60(9)
O(3)–Eu(1)–O(4D)	78.31(9)	O(4D)–Eu(1)–O(1W)	140.29(9)
O(4)–Eu(1)–O(4D)	138.76(1)	O(6B)–Eu(1)–O(1W)	66.89(9)
O(3D)–Eu(1)–O(6B)	146.04(9)	O(6)–Eu(1)–O(1W)	70.35(1)
O(3)–Eu(1)–O(6B)	91.36(9)	O(3D)–Eu(1)–O(1WD)	93.61(1)
O(4)–Eu(1)–O(6B)	132.98(9)	O(3)–Eu(1)–O(1WD)	147.07(9)
O(4D)–Eu(1)–O(6B)	74.43(8)	O(4)–Eu(1)–O(1WD)	140.29(8)
O(3D)–Eu(1)–O(6)	91.36(9)	O(4D)–Eu(1)–O(1WD)	70.60(9)
O(3)–Eu(1)–O(6)	146.04(9)	O(6B)–Eu(1)–O(1WD)	70.35(1)
O(4)–Eu(1)–O(6)	74.43(8)	O(6)–Eu(1)–O(1WD)	66.89(9)
O(4D)–Eu(1)–O(6)	132.98(9)	O(1W)–Eu(1)–O(1WD)	103.26(2)
O(1)–Eu(2)–O(1A)	80.48(1)	O(5A)–Eu(2)–O(5)	135.61(1)

O(1)–Eu(2)–O(2C)	87.57(9)	O(1)–Eu(2)–O(4)	73.69(9)
O(1A)–Eu(2)–O(2C)	150.56(9)	O(1A)–Eu(2)–O(4)	77.52(8)
O(1)–Eu(2)–O(2C)	150.56(9)	O(2C)–Eu(2)–O(4)	124.73(9)
O(1A)–Eu(2)–O(2D)	87.57(9)	O(2D)–Eu(2)–O(4)	77.50(8)
O(2C)–Eu(2)–O(2D)	114.27(1)	O(5A)–Eu(2)–O(4)	150.05(9)
O(1)–Eu(2)–O(5A)	129.10(9)	O(5)–Eu(2)–O(4)	51.64(8)
O(1A)–Eu(2)–O(5A)	86.91(9)	O(1)–Eu(2)–O(4A)	77.52(8)
O(2C)–Eu(2)–O(5A)	79.92(1)	O(1A)–Eu(2)–O(4A)	73.69(9)
O(2D)–Eu(2)–O(5A)	76.41(9)	O(2C)–Eu(2)–O(4A)	77.50(8)
O(1)–Eu(2)–O(5)	86.91(9)	O(2D)–Eu(2)–O(4A)	124.73(9)
O(1A)–Eu(2)–O(5)	129.10(9)	O(5A)–Eu(2)–O(4A)	51.64(8)
O(2C)–Eu(2)–O(5)	76.41(9)	O(5)–Eu(2)–O(4A)	150.05(9)
O(2D)–Eu(2)–O(5)	79.92(1)	O(4)–Eu(2)–O(4A)	142.01(1)

Symmetry code A: -*x*, *y*, 0.5-*z*; B: *x*, *y*, 1+*z*; C: -*x*, *y*, -1+*z*; D: -*x*, *y*, 1.5-*z*.

2.4 Figure S2 TGA traces of Eu−**BPDA** ranging from room temperature to 500 °C.

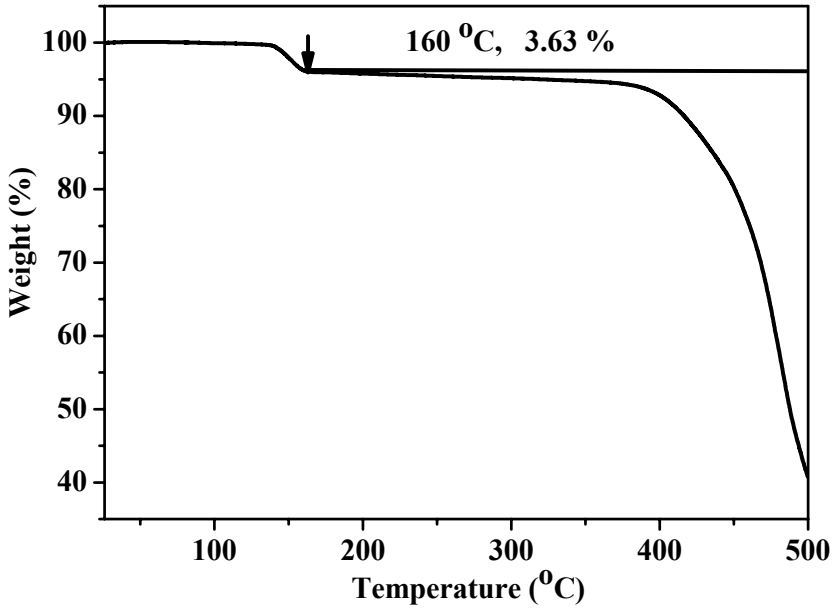

2.5 Figure S3 Powder XRD patterns of Eu−**BPDA** simulated from single-crystal X-ray diffraction results, the as-synthesized Eu−**BPDA** and Eu−**BPDA** treated with acetone and water.

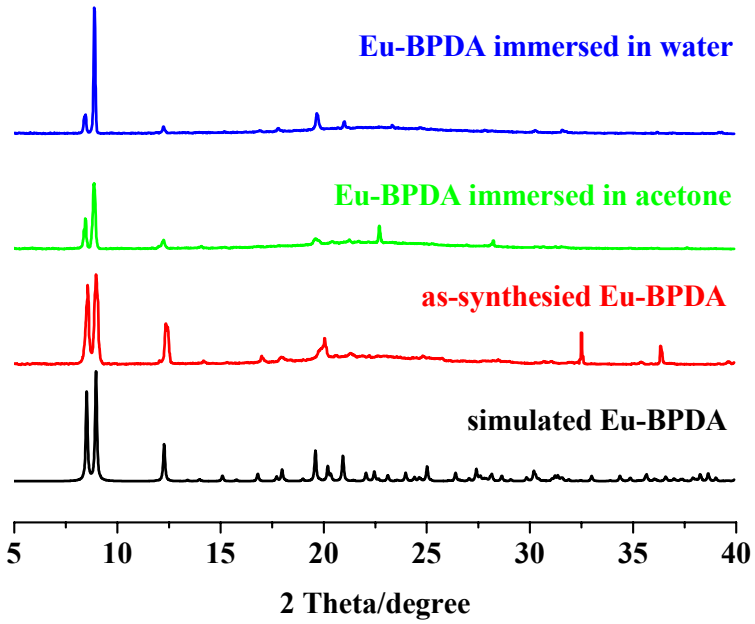

3. Recognition properties for small molecules based on Eu−BPDA.

3.1 Figure S4 The UV/vis absorption spectra for solid Eu−**BPDA**.

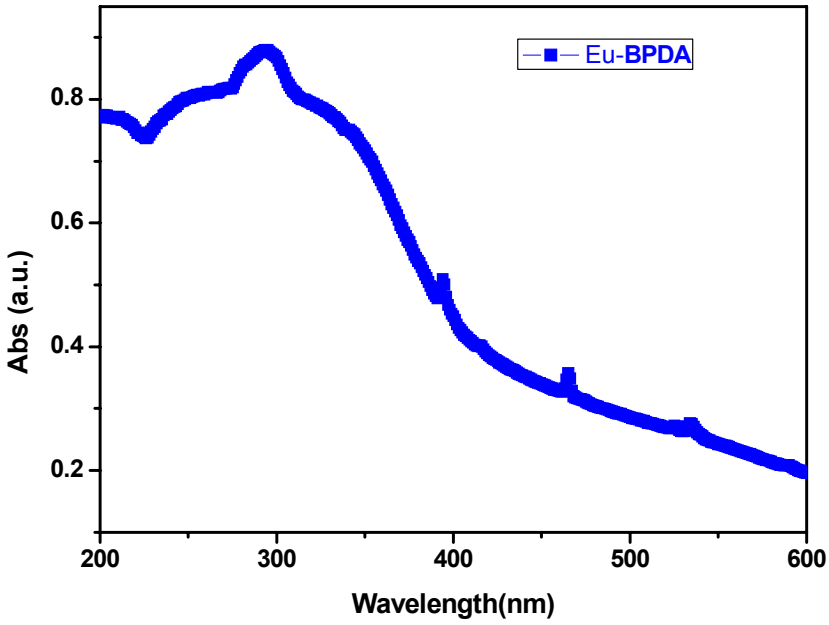

3.2 Figure S5 The fluorescence spectra of Eu−**BPDA** in methanol solvent when excited at 295 nm. The inset picture shows the two main bands arising from transitions from the emissive $^5D_0$ level to the $^7F_{1\text{-}4}$ levels of the ground states respectively.

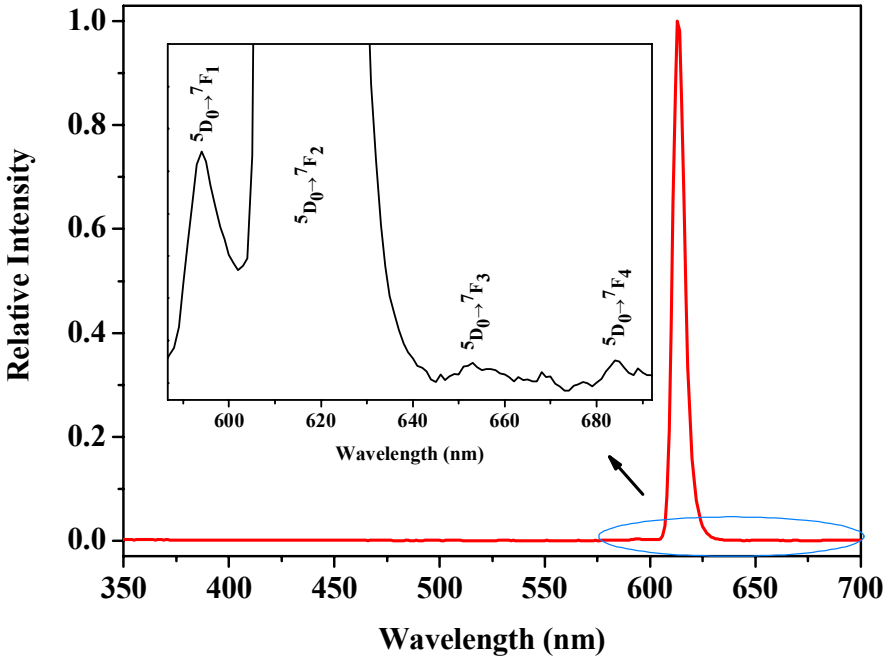

3.3 Figure S6 The fluorescence spectra of Eu−**BPDA** in various pure solvents when excited at 295 nm.

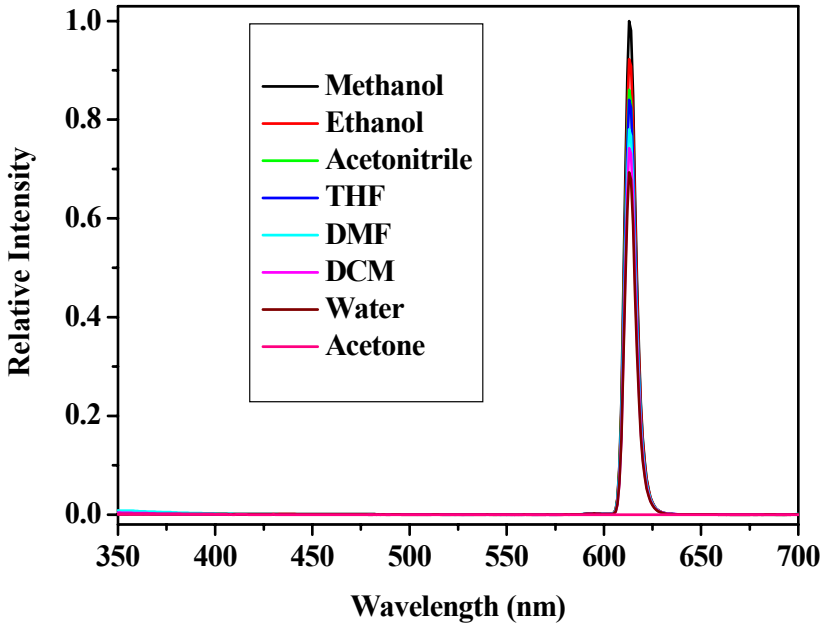

3.4 Figure S7 The fluorescence spectra of Eu−**BPDA** methanol emulsion as a function of acetone content.

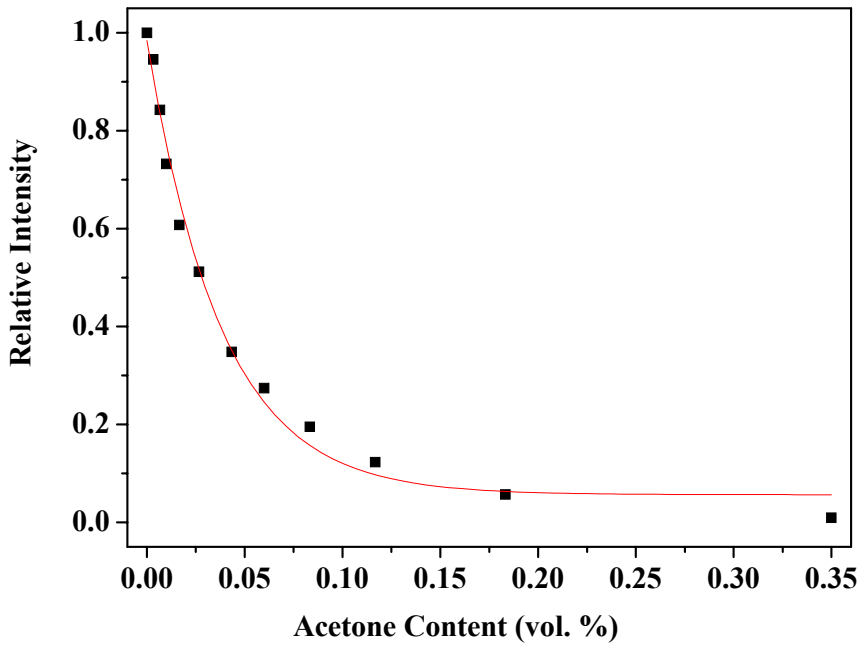

3.5 Figure S8 FT-IR spectra of Eu−**BPDA** and Eu−**BPDA** after immersed in acetone.

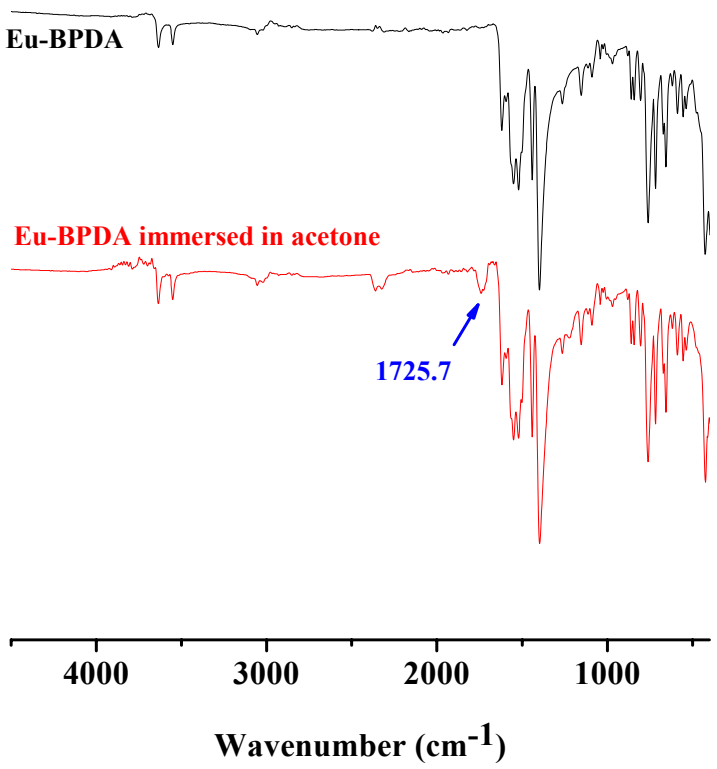

3.6 Figure S9 Study on recycling of Eu−**BPDA** for the fluorescence sensing of acetone in methanol solvent when excited at 295 nm.

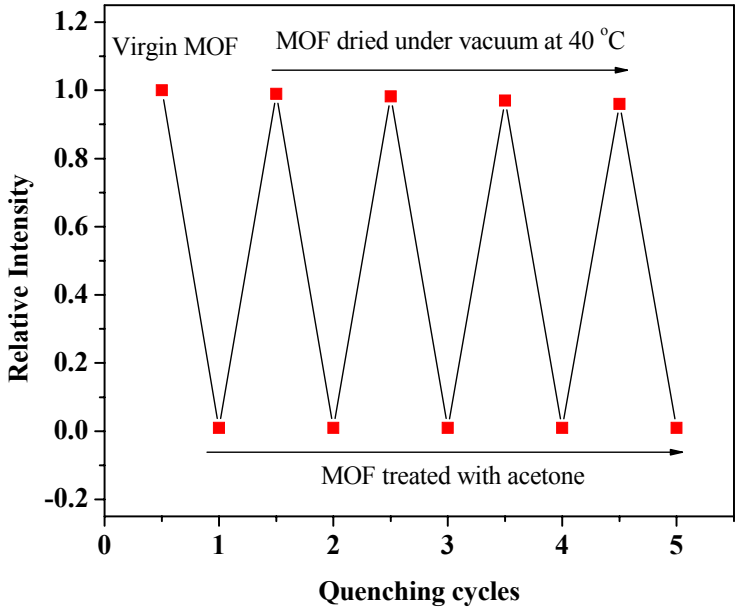

4. Recognition properties for metal ions based on Eu−BPDA

4.1 Figure S10 Family of fluorescence spectra of Eu−**BPDA** (0.6 mM) in water solution upon the addition of 1.8 mM of various metal ions.

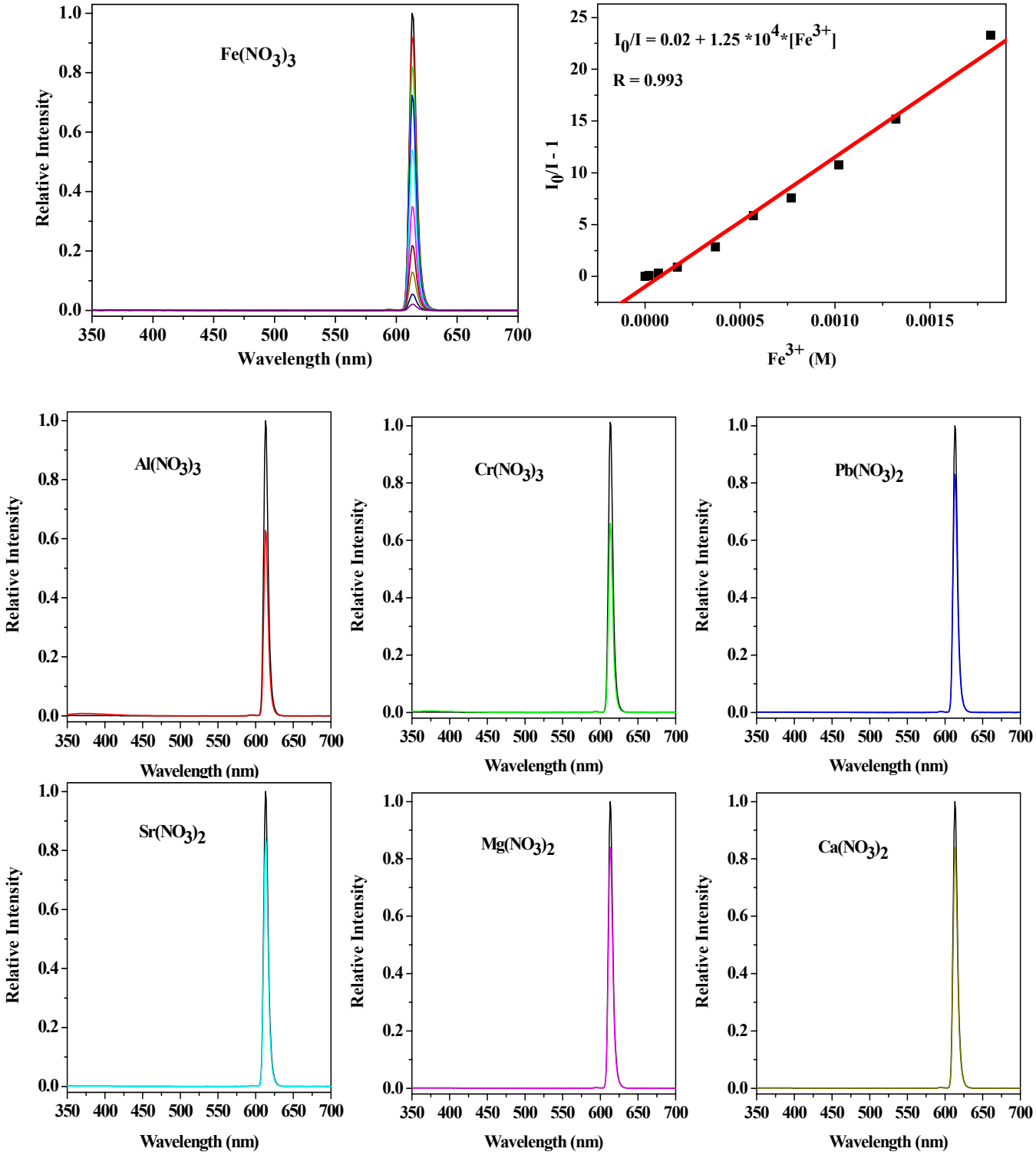

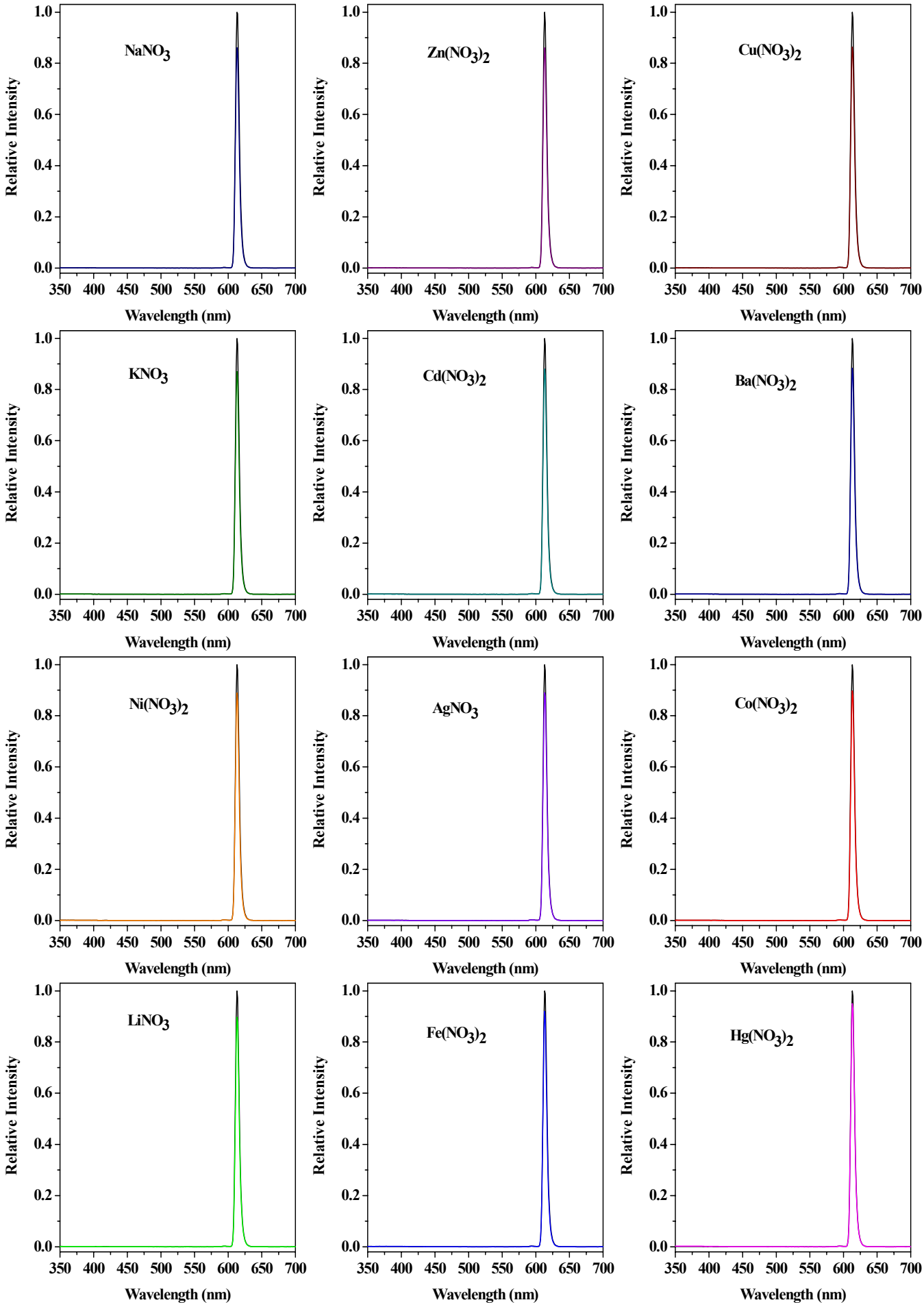
NaNO3
Zn(NO3)2
Cu(NO3)2
KNO3
Cd(NO3)2
Ba(NO3)2
Ni(NO3)2
AgNO3
Co(NO3)2
LiNO3
Fe(NO3)2
Hg(NO3)2
Relative Intensity
Wavelength (nm)
0.0
0.2
0.4
0.6
0.8
1.0
350
400
450
500
550
600
650
700